International Journal of Heat and Mass Transfer 52 (2009) 3738–3746

Contents lists available at ScienceDirect

International Journal of Heat and Mass Transfer

journal homepage: www.elsevier.com/locate/ijhmt

Experimental and numerical investigation of droplet evaporation under diesel engine conditions

C. Fieberg *, L. Reichelt, D. Martin, U. Renz, R. Kneer

Lehrstuhl für Wärme- und Stoffübertragung, RWTH Aachen University, D-52056 Aachen, Germany

ARTICLE INFO

Article history:
Received 28 July 2006
Received in revised form 7 November 2008
Accepted 19 January 2009
Available online 23 April 2009

Keywords:
Droplet evaporation
Transient Nusselt number
Drag coefficient

ABSTRACT

Evaporation of mono-disperse fuel droplets under high temperature and high pressure conditions is investigated. The time-dependent growth of the boundary layer of the droplets and the influence of neighboring droplets are examined analytically. A transient Nusselt number is calculated from numerical data and compared to the quasi-steady correlations available in literature. The analogy between heat and mass transfer is tested considering transient and quasi-steady calculations for the gas phase up to the critical point for a single droplet. The droplet evaporation in a droplet chain is examined numerically. Experimental investigations are performed to examine the influence of neighboring droplets on the drag coefficients. The results are compared with drag coefficient models for single droplets in a temperature range from T = 293–550 K and gas pressure p = 0.1–2 MPa. The experimental data provide basis for model validation in computational fluid dynamics.

© 2009 Elsevier Ltd. All rights reserved.

1. Introduction

Droplet breakup and evaporation in direct injection diesel engines govern the mixture formation process and thus determine combustion efficiency and pollutant formation. With characteristic evaporation times of a few milliseconds, the optimum parameter settings for the fuel injection are of crucial importance. Therefore, modeling of spray evaporation has become an indispensable tool for diesel engine development.

During the recent years Computational Fluid Dynamics (CFD) has become a standard means for combustion engine design and optimization. However, the simulation of the combustion process contains many physical phenomena where most of them are not well understood. The droplet breakup and evaporation processes are described by empirical correlations derived from global balances under steady-state conditions and it is questionable whether this approach is valid also for transient processes in an engine.

To gain insight into the evaporation and mixture formation processes, the interaction of the governing phenomena has to be considered. This can only be achieved by a detailed understanding of these phenomena.

Several authors investigated the interaction of droplets in a mono-disperse spray or droplet chain. Roth et al. [23] used Laser Doppler Anemometry (LDA) to measure droplet velocities in a mono-disperse droplet chain and also in a planar droplet array. To measure the droplet diameter during combustion they used a light scattering technique evaluating the resulting fringe pattern. During their investigations they found that the droplet deceleration in a single droplet chain is higher compared to a droplet chain array resulting in a higher drag coefficient for each droplet. In contrast, the burning rate increases for a single droplet chain as the oxygen concentration adjacent to the droplets is higher.

Anders et al. [3] used the same measurement techniques to evaluate the size and velocity of droplets in a mono-disperse droplet chain. They also showed that the droplet spacing is relevant for the combustion rate.

The interaction of droplets in a droplet chain and the influence on the drag coefficient were examined numerically and experimentally by Liu et al. [18]. They showed that the drag coefficient in a droplet chain is up to an order of magnitude smaller compared to a single droplet and verified their numerical results by corresponding measurements.

Most experiments were performed under ambient pressure conditions and including combustion. Therefore, this work is focused on the droplet evaporation of single droplets and mono-dispersed droplet chains under diesel engine conditions. The effect of the transient vapor phase composition is evaluated theoretically and the influence of the drag coefficient in a droplet chain is examined experimentally and numerically.

2. Droplet evaporation

Droplet evaporation in fuel sprays is usually described by empirical Nusselt and Sherwood laws derived from steady-state experiments with single droplets under subcritical conditions,

* Corresponding author. Tel.: +49 172 245 1532.
E-mail addresses: cfieberg@gmx.de (C. Fieberg), lars.reichelt@arcor.de (L. Reichelt).

0017-9310/$ - see front matter © 2009 Elsevier Ltd. All rights reserved.
doi:10.1016/j.ijheatmasstransfer.2009.01.044

Nomenclature

c_p	heat capacity (J/kg K)	c_D	drag coefficient
D	diffusion coefficient (m^2/s)	Fo	Fourier number ($=\alpha t/d^2$)
d	droplet diameter (m)	Le	Lewis number (=Pr/Sc)
F	force (N)	B_M	mass transfer number
h	heat transfer coefficient (W/m^2 K)	B_T	heat transfer number
k	thermal conductivity (W/m K)	Nu	Nusselt number ($=hd/k$)
g	mass transfer coefficient (kg/m^2 s)	Pr	Prandtl number ($=\eta c/k$)
$\dot{m}$	mass flux (kg/s)	Re	Reynolds number ($=d\varrho u/\eta$)
p	pressure (MPa)	Sc	Schmidt number ($=\eta/D\varrho$)
$\dot{Q}$	heat flux (W)	Sh	Sherwood number ($=gd/\varrho D$)
r	radial coordinate (m)	We	Weber number ($=d\varrho u^2/\sigma$)
R	droplet radius (m)	ad	adiabatic
s	Laplace variable (dimensionless)	∞	ambient
t	time (s)	crit	critical condition
u	velocity (m/s)	d	droplet
z	dimensionless radius (dimensionless)	g	gas
α	thermal diffusivity ($=k/\varrho c$, m^2/s)	l	liquid
Δx	droplet spacing (m)	M	mass transfer
Δh_v	heat of vaporization (J/kg)	ref	reference
η	dynamic viscosity (kg/m s)	rel	relative
κ	correction factor (dimensionless)	s	surface
ϱ	density (kg/m^3)	T	heat transfer
σ	surface tension (kg/s^2)	0	initial
τ	dimensionless time (dimensionless)	1	first droplet
Θ	dimensionless temperature (dimensionless)	2	second droplet
ξ	mass concentration (dimensionless)	eff	effective

e.g. [20,11]. For Le = Pr/Sc≠1 [1] suggested a modified correlation to include variable properties and deviations from the analogy between heat and mass transfer.

Miller et al. [19] compared evaporation models following the Langmuir–Knudsen law with experimental data and found no significant deviations for low evaporation rates. Considering higher evaporation rates, non-equilibrium effects lead to a strong variation in the models.

The influence of neighboring droplets on the effective mass transfer number B_M and the heat transfer number B_T is evaluated numerically by [8]. They examined two droplets in a tandem position in a hot gas environment and the following correlations are given for the second droplet:

$$\begin{aligned}\frac{\mathrm{Nu}}{\mathrm{Nu}_0} &= 0.549\,\mathrm{Re}^{-0.146}\,\mathrm{Pr}^{-0.768}(1+B_T)^{0.356}\Delta x^{0.262}\left(\frac{d_2}{d_1}\right)^{0.147},\\ \frac{\mathrm{Sh}}{\mathrm{Sh}_0} &= 0.974\,\mathrm{Re}^{0.127}\,\mathrm{Sc}^{-0.318}(1+B_M)^{-0.363}\Delta x^{-0.064}\left(\frac{d_2}{d_1}\right)^{0.857}.\end{aligned} \tag{1}$$

with the definition of B_M and B_T:

$$\begin{aligned}B_M &= \frac{\xi_s-\xi_\infty}{1-\xi_s},\\ B_T &= c_p(T_\infty - T_s)\left(1-\frac{\dot{Q}_l}{\dot{Q}_g}\right)\frac{1}{\Delta h_v}.\end{aligned} \tag{2}$$

The Nusselt and Sherwood correlations Nu_0 and Sh_0 are given as

$$\begin{aligned}\mathrm{Nu}_0 &= 1.275\,\mathrm{Re}^{0.438}\,\mathrm{Pr}^{0.619}(1+B_T)^{-0.678},\\ \mathrm{Sh}_0 &= 1.224\,\mathrm{Re}^{0.385}\,\mathrm{Sc}^{0.492}(1+B_M)^{-0.568}.\end{aligned} \tag{3}$$

The correlations of Eq. (1) describe the evaporation in fuel sprays and mono-disperse sprays in a detailed manner. Here, the effect of the lead droplet changes the evaporation history of the second droplet compared with an isolated one. This correlation also includes the effects of droplet spacing and changing flow field.

3. Evaporation models

3.1. Evaporation under steady-state conditions

As mentioned above, droplet evaporation is usually described by Nusselt and Sherwood correlations from steady-state experiments with fully developed thermal and vapor boundary layers. This is a severe constriction concerning the simulation of droplet evaporation in diesel engines.

Usually, for ambient temperatures and pressures, a simple evaporation model is considered. The heating of the droplet to the adiabatic evaporation temperature T_{ad} and the evaporation are modeled as consecutive processes. Assuming, analogy between heat and mass transfer (Le = Pr/Sc = 1), the adiabatic temperature at low Reynolds numbers is

$$T_{ad} = T_g - \frac{\Delta h_v}{c_{p,g}}B_M. \tag{4}$$

The droplet evaporation in terms of surface decrease follows a linear function (d^2-law):

$$\left(\frac{d}{d_0}\right)^2 = 1 - \frac{8k_g}{\varrho_d c_{p,g} d_0^2}\ln(1+B_M)t. \tag{5}$$

The resulting evaporation time under these conditions is

$$t_{ev} = d_0^2\frac{\varrho_d c_{p,g}}{8k_g\ln(1+B_M)}. \tag{6}$$

Under diesel engine conditions, these assumptions are no longer valid and a detailed evaluation of the evaporation model has to be considered.

3.2. Transient evaporation

The evaporating droplets develop a boundary layer while the evaporation takes place. Furthermore, the ambient conditions for

each droplet vary with time due to droplet velocity, vapor concentration and the interaction with other droplets (transient gas phase). Thus, the Nusselt number for each droplet varies with space and time.

In this section, several simple models are used to estimate the effect of fast evaporation and transient boundary layers on the evaporation process and the time averaged Nusselt and Sherwood numbers. From this, it can be concluded whether the steady-state correlations may be used for the numerical simulation or if more sophisticated correlations have to be developed and deployed.

The life time of a droplet under diesel engine conditions is in the order of milliseconds, Eq. (6). Therefore, the assumption of a quasi-steady evaporation is questionable.

To evaluate the deviation of the quasi-steady solution from the transient one, a time averaged Nusselt number is evaluated from a transient analytical calculation. As a simplification, the coupling between heat and mass transfer is neglected and only the heat transfer will be considered.

To find an analytical solution of the partial differential equation for conservation of energy, the heat transfer from hot gas to a single droplet in a quiescent ambient without relative gas velocity is considered. Thus, the heat transfer is purely driven by conduction ($\mathrm{Re}\times\mathrm{Pr}\ll 1$). Furthermore, spherical symmetry is assumed and the dependent variable (temperature) is only a function of the radial distance from the droplet center and time.

The energy balance for the ambient gas ($t=0: T=T_\infty$) in which a droplet with temperature T_d and radius $R(t)$ is exposed can be formulated as

$$\frac{\partial T}{\partial t}=\alpha\frac{1}{r^2}\frac{\partial}{\partial r}\left(r^2\frac{\partial T}{\partial r}\right) \tag{7}$$

with initial and boundary conditions

$$\begin{aligned} &T(t=0, r\geqslant R)=T_\infty,\\ &T(t>0, r=R)=T_\mathrm{d},\\ &T(t>0, r\to\infty)=T_\infty. \end{aligned} \tag{8}$$

To yield the transient temperature field, the differential equation (7) is solved using Laplace transformation (see Appendix A). From the temperature gradient at the droplet surface, the transient Nusselt number is calculated as a function of the Fourier number (see Eq. A.10):

$$\mathrm{Nu}=\frac{hd}{k}=\frac{d}{T_\infty-T_\mathrm{d}}\left.\frac{\partial T}{\partial r}\right|_{r=R}=2+\frac{1}{\sqrt{\pi\,\mathrm{Fo}_0}},\quad \mathrm{Fo}_0=\frac{\alpha t}{d_0^2}. \tag{9}$$

For large Fourier numbers ($\mathrm{Fo}_0\to\infty$), Eq. (9) yields the well-known correlation $\mathrm{Nu}=2$. The time averaged Nusselt number follows from integration of Eq. (9)

$$\overline{\mathrm{Nu}}=\frac{1}{\mathrm{Fo}_0}\int_0^{\mathrm{Fo}_0}\mathrm{Nu}\,d\widetilde{\mathrm{Fo}_0}=2\left(1+\frac{1}{\sqrt{\pi\,\mathrm{Fo}_0}}\right). \tag{10}$$

The dimensionless time for evaporation analog to Eq. (6) is

$$\mathrm{Fo}_{0,\mathrm{ev}}=\frac{1}{8\ln(1+B_\mathrm{M})}\frac{\varrho_\mathrm{d}}{\varrho_\mathrm{g}}. \tag{11}$$

By inserting $\mathrm{Fo}_{0,\mathrm{ev}}$ in Eq. (10), the mean Nusselt number during the evaporation process is given as

$$\overline{\mathrm{Nu}_\mathrm{ev}}=2\left(1+\sqrt{\frac{8\ln(1+B_\mathrm{M})}{\pi}\frac{\varrho_\mathrm{g}}{\varrho_\mathrm{d}}}\right). \tag{12}$$

It should be remembered that this Nusselt number does neither consider the decreasing diameter nor the heating up prior to evaporation. Thus, it is only a rough estimation. The effective Nusselt number will be smaller than the estimated one.

Fig. 1 shows the time averaged Nusselt numbers of evaporating *n*-dodecane droplets at different pressures and temperatures (left) and the corresponding adiabatic droplet temperatures (right). The vapor pressure for the effective mass transfer number B_M is calculated from Gmehling and Kolbe [12].

The results show that the mean Nusselt number for diesel engine conditions ($T_\mathrm{g}>700$ K, $p_\mathrm{g}>5$ MPa) is above 2.5. From this result is it not possible to decide whether the transient effects may be neglected. The value of 2.5 suggests that the transient effects may not be neglected, but since the Nusselt number is overestimated (as shown later), the coupled heat and mass transfer for a single droplet is investigated numerically in the following section.

3.2.1. Numerical investigation on single droplet evaporation

The time-dependent conservation equations for energy and mass for a single spherical droplet in dimensionless form ($z=r/R$) are (Appendix B):

$$\begin{aligned} &\frac{\partial T}{\partial t}-\left(z\frac{\dot R}{R}+\frac{2\alpha}{zR^2}\right)\frac{\partial T}{\partial z}-\frac{\alpha}{R^2}\frac{\partial^2 T}{\partial z^2}=0,\\ &\frac{\partial \xi_i}{\partial t}-\left(z\frac{\dot R}{R}+\frac{2D}{zR^2}\right)\frac{\partial \xi_i}{\partial z}-\frac{D}{R^2}\frac{\partial^2 \xi}{\partial z^2}=0. \end{aligned} \tag{13}$$

The conservation equations for the gas phase have a similar structure, but include an additional convective term due to the Stefan flow

$$\begin{aligned} &\frac{\partial T}{\partial t}-\left(z\frac{\dot R}{R}-\frac{\dot m''}{z^2\varrho R}+\frac{2\alpha}{zR^2}\right)\frac{\partial T}{\partial z}-\frac{\alpha}{R^2}\frac{\partial^2 T}{\partial z^2}=0,\\ &\frac{\partial \xi_i}{\partial t}-\left(z\frac{\dot R}{R}-\frac{\dot m''}{z^2\varrho R}+\frac{2D}{zR^2}\right)\frac{\partial \xi_i}{\partial z}-\frac{D}{R^2}\frac{\partial^2 \xi}{\partial z^2}=0, \end{aligned} \tag{14}$$

with the evaporating surface mass flux $\dot m''$ and the temporal derivative of the droplet radius $R, \dot R$:

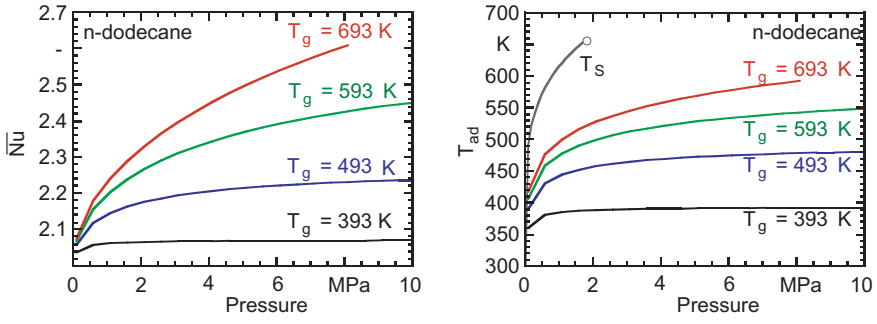

Fig. 1. Time averaged Nusselt number of a evaporating droplet, $u_\mathrm{g}=0$ m/s and corresponding adiabatic temperatures. Curve T_S shows the boiling temperature.

Table 1
Comparison of the models used for the simulation of the droplet evaporation.

	Model	Liquid phase	Gas phase
1	Hohmann [13]	Transient, temperature and space dependent properties	1/3 rule, Eq. (17)
2	New quasi-steady model		Quasi-steady, temperature and space dependent properties
3	New transient model		Transient, temperature and space dependent properties

$$\dot{m}'' = \frac{\dot{m}}{4\pi R^2}, \quad \dot{R} = \frac{dR}{dt}. \tag{15}$$

For quasi-steady conditions in the gas phase, Eq. (14) is simplified to

$$\left(-\frac{\dot{m}''}{z^2\varrho R} + \frac{2\alpha}{zR^2}\right)\frac{\partial T}{\partial z} + \frac{\alpha}{R^2}\frac{\partial^2 T}{\partial z^2} = 0,$$
$$\left(-\frac{\dot{m}''}{z^2\varrho R} + \frac{2D}{zR^2}\right)\frac{\partial \xi_i}{\partial z} + \frac{D}{R^2}\frac{\partial^2 \xi_i}{\partial z^2} = 0. \tag{16}$$

The numerical simulation of droplet evaporation including real gas effects such as solubility and thermal properties for super- and subcritical conditions are implemented in a software code based on the work of [13,14,16]. For the analysis of droplet evaporation, three different models are used. These are summarized in Table 1 and discussed in detail below. In all models, the properties of the droplet phase are computed for each time-step based on the local droplet temperature and composition. Correlations given by [22,9] are used to calculate local density, thermal conductivity and diffusivity.

Hohmann [13] (Model 1 in Table 1) assumes a quasi-steady gas phase and calculates the heat and mass transfer using corrections from Abramzon and Sirignano [1] for non-constant properties and deviations from the analogy between heat and mass transfer, i.e. Le = Pr/Sc≠1. The thermophysical properties for the gas phase are calculated with a reference temperature suggested by [15] (so-called 1/3 rule).

$$T_{\mathrm{ref}} = \frac{2}{3}T_s + \frac{1}{3}T_\infty. \tag{17}$$

The conservation equations for the droplet interior (13) are solved with variable thermophysical properties. The fluid circulation within the droplet (hill vortex) is taken into account by an effective conductivity and an effective diffusivity:

$$k_{\mathrm{eff}} = \kappa \cdot k, \quad D_{\mathrm{eff}} = \kappa \cdot D. \tag{18}$$

The correction factor κ is given by the effective conductivity model of [1] and is a function of Reynolds and Prandtl number and the viscosity ratio of gas and droplet.

The second model used in the computations also assumes a quasi-steady gas phase, but uses local, transient thermophysical properties. Heat and mass transfer are computed from the temperature and vapor concentration gradients at the droplet surface. In the third model, a transient computation of the gas phase is performed using local properties.

A comparison of the three models is shown in Fig. 2 for the evaporation of a *n*-heptane droplet with an initial diameter of 50 μm in an environment with initial temperature of 700 K and pressure of 7 MPa. The critical pressure and temperature of *n*-heptane are 2.7 MPa and 540 K, respectively. The upper plot shows the normalized surface area of the droplet and the droplet surface temperature versus time.

There is very good agreement between the quasi-steady computations using local properties and the one with averaged properties using the 1/3-rule. The fully transient computations (model 3)

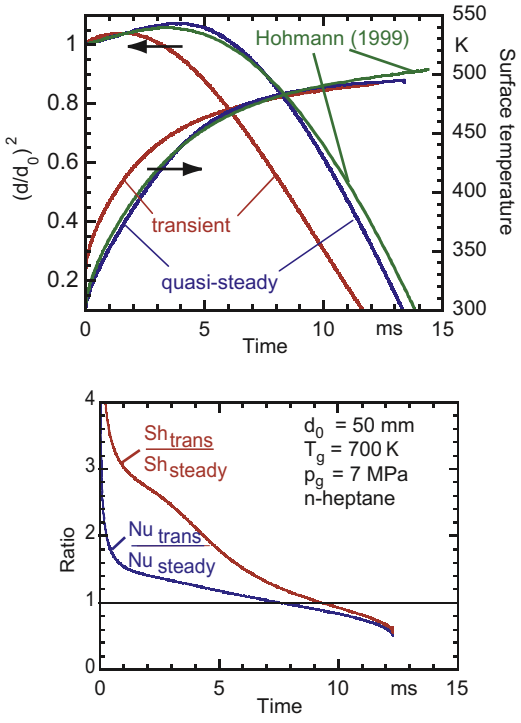

Fig. 2. (top) Comparison of droplet diameter and surface temperature. (bottom) Ratio of Nusselt and Sherwood numbers for transient and quasi-steady models.

show a faster initial heating of the droplet, but the difference in droplet life time is less than 10 %. This is in accordance with results from [2]. It can be seen that the initial decrease of the droplet diameter is faster than in the quasi-steady computations, but for times larger 7 ms the quasi-steady computations show faster evaporation resulting in similar evaporation times.

The cause of this effect is shown in the lower part of Fig. 2. Here, the ratio of the Nusselt and Sherwood numbers from models 2 and 3 are plotted versus time. As expected from the simple model, Eq. (9), Nusselt and Sherwood numbers are very large at the beginning. As the boundary layers develop, the transient Nusselt and Sherwood numbers decrease below the quasi-steady value. The reason for this is illustrated in Fig. 3.

Here, the temperature distributions in the droplet and the gas phase for the transient and quasi-steady model are shown. The scale of the abscissa is different for the droplet and the surrounding gas. As expected, the initial temperature gradients are steeper in case of transient calculations and thus are the heat and mass transfer rates. During the evaporation process, the boundary layers increase because of the rapid diameter reduction and slow down the exchange process between droplet surface and the adjacent gas phase. The conservation equations (13) and (14) confirm this result and show an increase of the convective term $\dot{R}/R$ which causes the growth of the boundary layer.

The mean values of the ratio of transient to steady-state Nusselt numbers from Fig. 2 is about 1.2. The effect of the very large initial Nusselt numbers is attenuated by the decreasing Nusselt numbers at the end of the droplet life time. These computations show that the simple model neglecting the coupling of heat and mass transfer overestimates the effect of transient evaporation.

The calculations show that the quasi-steady models for the gas phase are sufficiently exact to model the overall evaporation of fuel droplets for a wide range of temperature and pressure. Further investigation is needed to determine whether the different evaporation rates in the beginning of evaporation have a significant effect on the ignition of fuel sprays.

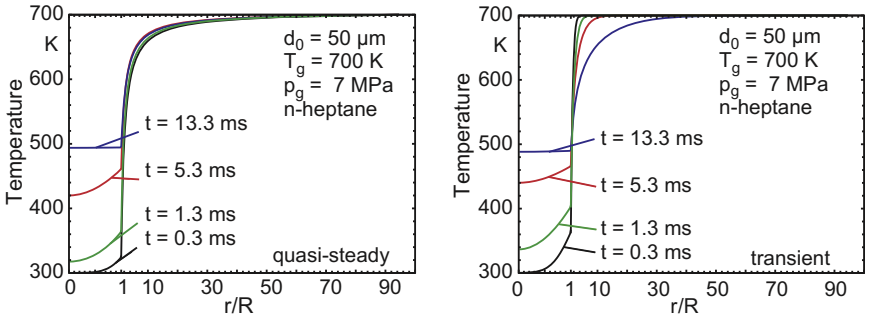

Fig. 3. Comparison of the temperature profile in droplet and gas phase for different times. (left) Quasi-steady; (right) transient profiles.

4. Droplet interaction

The number of droplets in fuel sprays in an internal combustion engine is very high and leads to interaction between the droplets. Numerical and experimental studies of a mono-disperse droplet chain were carried out to demonstrate the influence on momentum exchange. The droplet chain provides well-defined spacings and velocity distribution between the droplets to isolate different physical effects and is often used in experimental setups, e.g. [23,3].

4.1. Numerical studies

The flow field around 10 droplets of a monodisperse droplet chain is investigated using the CFD program FLUENT 6.0 [10]. To simplify the computations, the droplets where assumed to be stagnant while being exposed to a gas stream with velocity u_∞. From the forces acting on the droplet surfaces, the drag coefficients c_D are calculated using Eq. (19) and the free stream velocity u_∞. The values are compared to data for single droplets.The calculations are performed using a two-dimensional unstructured mesh. The boundary layer around the droplets was resolved with rectangular cells with a thickness of 2 µm. The number of cells was in the range from 6000 to 22,000 depending on the droplet spacing and thus the length of the domain. At the outer edge of the domain at $R = 0.5\ \text{mm} = 5d$, a wall with free-slip condition was set.

Since the Reynolds number $\text{Re} = d\varrho u_\infty/\eta$ is in the range $\text{Re} < 140$ laminar flow is assumed.

Fig. 4 displays the velocity field around the droplets for a Reynolds number of $\text{Re} = 70$ and different dimensionless droplet spacings. The Reynolds number is calculated using the initial droplet diameter d_0 and the gas velocity at the domain inlet u_∞.

With decreasing droplet spacing, the gas velocity between the droplets also decreases strongly. By integrating the forces acting on the droplet, the drag coefficient is computed for each droplet:

$$c_D = \frac{F}{u_\infty^2}\frac{8}{\pi d^2 \varrho_g}. \tag{19}$$

These results are in good qualitative agreement with numerical and measured data from [18]. A direct comparison is not possible as the authors only present data for one Reynolds number ($\text{Re} = 10$), whereas the investigation in this paper focusses on higher Reynolds numbers.

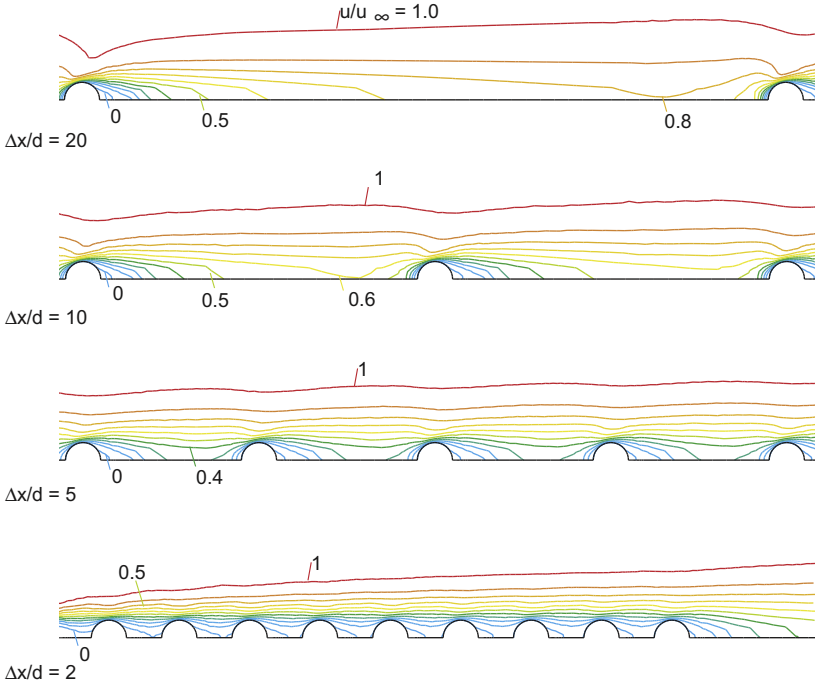

Fig. 4. Gas velocity between the droplets of a droplet chain, $\text{Re} = 70$, $d = 100$ µm.

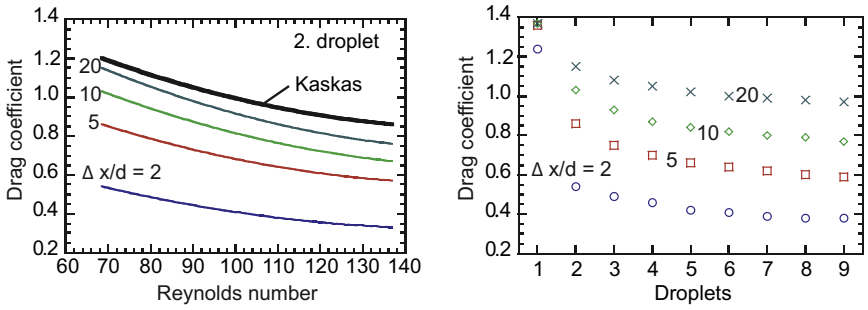

Fig. 5. Drag coefficients in a droplet chain. (left) Influence of droplet spacing on the drag coefficient of the second droplet. (right) Specific drag coefficient of the droplets in the droplet chain for Re = 70.

The drag coefficient for a single droplet as a function of Reynolds number is given by Kaskas (e.g. [5]) as

$$c_D = \frac{24}{Re} + \frac{4}{\sqrt{Re}} + 0.4. \tag{20}$$

The effect of the droplet spacing on the drag coefficient is shown in Fig. 5. On the left-hand side, the drag coefficient for the second droplet is plotted versus Reynolds number for different dimensionless spacings $\Delta x/d$. Even for a relative wide spacing of $\Delta x/d = 20$, an influence from the leading droplet is still visible. Furthermore, the drag coefficients decrease from droplet to droplet and are 30% below the value of the droplets in front, as shown in Fig. 5 (right) for a Reynolds number of 70.

4.2. Experimental setup

A droplet chain of iso-octane with initial droplet sizes from $d_0 = 90–120\ \mu m$ and initial velocities $v_0 = 9–15$ m/s is injected into a heated pressurized chamber with gas pressures $p_g = 0.1–3.7$ MPa and ambient temperatures $T_g = 300–550$ K. A schematic sketch of the pressurized chamber is shown in Fig. 6.

The droplet velocities and diameters are measured with Phase-Doppler Anemometry (PDA) at different positions downstream of the nozzle. The detectors for the scattered laser light were set up at an angle of $\varphi = 65^\circ$ to the forward direction. Thus, the dependence of the PDA signal on the refractive index is very small [17] and the droplet temperature does not affect the diameter measurements.

The drag coefficient for the droplets in the chain is calculated from the velocity measurements and the gradient in the velocity profile neglecting gravitational force, Eq. (22). The gas velocity is considered to be zero.

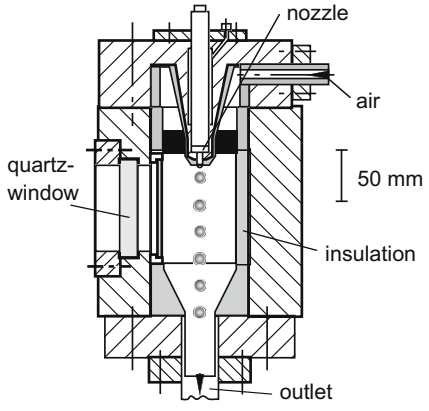

Fig. 6. Schematic sketch of the pressurized chamber taken from [24].

$$\varrho_d \frac{\pi}{6} d^3 \frac{d\vec{u}}{dt} = c_D \frac{\pi}{8} d^2 \varrho_g \vec{u}|\vec{u}|, \tag{21}$$

$$\frac{d\vec{u}}{dt} = \frac{3}{4} \frac{\varrho_g}{\varrho_d} \frac{\vec{u}|\vec{u}|}{d} c_D. \tag{22}$$

The droplet acceleration is not directly measurable with the PDA setup, but from the droplet velocity profile versus distance from the nozzle it is possible to gain the spatial velocity gradient for insertion into Eq. (22) and solve for c_D:

$$c_D = -\frac{4}{3} \frac{\varrho_d}{\varrho_g} \frac{d}{\tilde{u}} \frac{d\tilde{u}}{dx}, \quad \tilde{u} = \frac{u}{u_0}. \tag{23}$$

To reduce noise from the experimental data, the velocity profile is approximated by an exponential function $u(x) = c_1 \exp(-c_2 x)$ as shown in Fig. 7.

The resulting drag coefficients c_D for droplet chains are nearly constant in the examined Reynolds number regime and significantly below the values of c_D for single droplets calculated by Eq. (20). This is consistent with the results of Liu et al. [18] who showed in their investigations that the drag coefficient for a droplet in a droplet chain is up to an order of magnitude smaller than the drag coefficient of a single droplet in an unconfined parallel flow.

The dimensionless distance between the droplets was varied from $1.8 \leqslant \Delta x/d \leqslant 2.2$ due to limitations of the droplet generator used. The droplets were generated using controlled Rayleigh break-up of a liquid jet excited by a piezoceramic disk. The orifice has got a diameter of 50 μm. The influence of droplet diameter and droplet spacing between the droplets in the chain is very low in the examined range. For a gas density $\varrho_g = 12.8$ MPa and two different temperatures, the drag coefficient is in the range of $0.3 \leqslant c_D \leqslant 0.4$ and in good agreement with the calculated drag coefficients from the FLUENT simulations for a droplet spacing of $\Delta x/d = 2$, Fig. 8.

Since there is no secondary droplet break-up nor chemical reaction in the pressurized chamber, the decrease in droplet size is caused by evaporation only. Liu et al. [18] found the following correlation for a stable droplet in a droplet chain:

$$We = \frac{\varrho_g u_{rel}^2 d}{\sigma} \leqslant We_{crit} \approx \frac{80}{c_D}. \tag{24}$$

The measurements are therefore limited to small Weber numbers ($We < 80$) and moderate temperatures. For higher temperatures ($T_g > 550$ K), self ignition of the fuel droplets yields an additional evaporation effect and is not investigated here.

Castanet et al. [7] examined a combusting droplet chain at atmospheric pressures. Using an electrostatic deviator they removed droplets from the droplet chain and were thus able to vary the dimensionless distance in a wider range $2 \leqslant \Delta x/d \leqslant 18$. Their results show that the Nusselt and Sherwood numbers decrease for dimensionless distances of $\Delta x/d < 6$ and are constant for larger

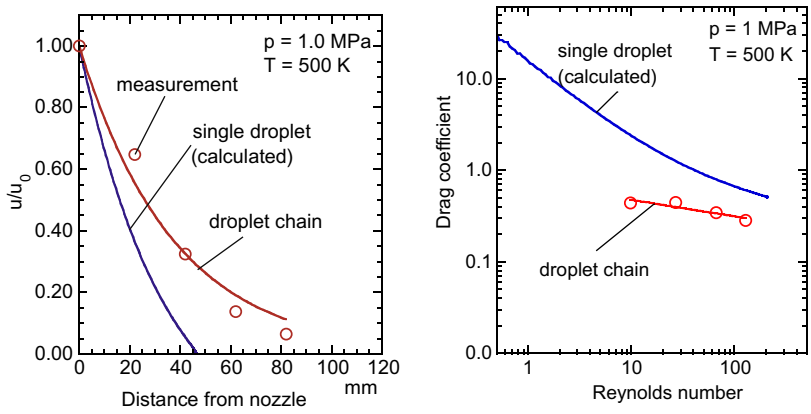

Fig. 7. Comparison of velocities (left) and drag coefficients (right) between droplet chain ($\Delta x/d \approx 2$) and single droplet.

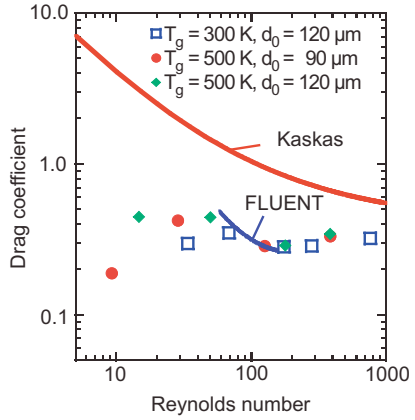

Symbol	$d[\mu m]$	$\Delta x/d$ [-]	T [K]	p [MPa]
□	120	4	300	1.0
●	90	2	500	1.7
♦	120	4	500	1.7

Fig. 8. Influence of temperature and droplet distance on the drag coefficient.

distances. The Reynolds numbers were in the range of $14 < Re < 45$. From the diagrams, drag coefficients can be estimated showing similar results as in the present study.

Roth et al. [23] also showed that the droplet deceleration in a droplet chain is much smaller compared to a single droplet. Furthermore, the burning rate of single droplets is higher because of more available oxygen.

Since spray formation and penetration are strongly influenced by interactions between liquid and gaseous phase the dependence of the drag coefficient on the droplet distance has to be considered in numerical computations. Most models in commercial CFD codes include non-spherical droplet shapes in the calculation of the drag coefficient, but only few models consider droplet interaction. Thus, for precise prediction of spray behavior new and more sophisticated models have to be developed.

Besides the number density of the droplets in the flow field, the grid size and time steps have to be considered because simulations of dense sprays with the Euler–Lagrange method and small grid cells produce grid-dependent results (e.g. [21]).

5. Conclusions

Droplet evaporation and interaction have been analyzed using numerical and experimental methods. For the numerical investigations, an existing program has been extended to allow fully transient computations. The calculations show good agreement for the droplet life time, although the time-dependent evolution of the droplet diameter for a transient and a quasi-steady consideration of the gas phase differ obviously. The reason for this difference is due to the additional convective term in the conservation equations which increases extremely compared to the other terms during the evaporation process. This results in a thicker boundary layer and thus in a reduced heat and mass exchange between gas and droplet. The time averaged Nusselt number during the droplet life time is slightly higher than the Nusselt number for a quasi-steady gas phase.

The numerical results show that evaporation calculations in engine applications using quasi-steady modeling of the gas phase are valid even for super critical conditions and produce acceptable errors compared to a fully transient calculation. Since the evaporation takes place in a spray plume, the surrounding gas is cooled below the critical temperature and only a small number of droplets evaporate under super critical conditions. The effect on the whole spray is thus further reduced.

Drag coefficients in droplet chains are examined experimentally in a pressurized chamber with temperatures up to $T_g = 550$ K and pressures up to $p_g = 1.8$ MPa. The drag coefficients computed numerically correlate well with the measured values. Experiments and numerical results show a strong interaction of the droplets in a mono-disperse droplet chain. The drag coefficients in a droplet chain are weakly correlated to the Reynolds number. Even for wide droplet spacings of $\Delta x/d = 20$ an interaction is still visible, but in this the considerations of a single droplet would be more likely.

Next to the momentum exchange, the evaporation in droplet chains should be investigated experimentally to have a sound basis for evaluating the presented models.

The models for the simulation of dense sprays in combustion engines have to be modified to include the effect of interacting droplets on the drag coefficient.

Appendix A. A solution of the differential equation (7)

The differential equation (7) with initial and boundary conditions (8) can be solved using the Laplace transformation. Introducing new variables

$$\Theta = \frac{T - T_\infty}{T_d - T_\infty}, \quad z = \frac{r}{R}, \quad \tau = \frac{t\alpha}{R^2} \tag{A.1}$$

gives

$$\frac{\partial \Theta}{\partial \tau} = \frac{1}{z^2}\frac{\partial}{\partial z}\left(z^2 \frac{\partial \Theta}{\partial z}\right) \tag{A.2}$$

with new initial and boundary conditions:

$$\begin{aligned}&\Theta(\tau=0,\ z\geqslant 1)=0,\\&\Theta(\tau>0,\ z=1)=1,\\&\Theta(\tau>0,\ z\to\infty)=0.\end{aligned}\tag{A.3}$$

By using the Laplace transformation, the partial differential equation can be transformed into an ordinary differential equation with new boundary conditions:

$$\begin{aligned}&\frac{1}{z^2}\frac{d}{dz}\left(z^2\frac{d\bar{\Theta}}{dz}\right)=s\bar{\Theta},\\&\bar{\Theta}(z=1)=\frac{1}{s},\\&\bar{\Theta}(z\to\infty)=0.\end{aligned}\tag{A.4}$$

Substituting $\phi=z\bar{\Theta}$ yields

$$\frac{d^2\phi}{dz^2}-s\phi=0\tag{A.5}$$

with the well-known general solution

$$\begin{aligned}&\phi=z\bar{\Theta}=C_1e^{z\sqrt{s}}+C_2e^{-z\sqrt{s}},\\&\bar{\Theta}=\frac{C_1e^{z\sqrt{s}}+C_2e^{-z\sqrt{s}}}{z}.\end{aligned}\tag{A.6}$$

The constants C_1 and C_2 are found from the boundary conditions:

$$\bar{\Theta}=\frac{e^{(1-z)\sqrt{s}}}{sz}.\tag{A.7}$$

For the calculation of the transient Nusselt number, only the gradient of the temperature at the droplet surface is needed. Thus, the gradient may be computed before the result is transformed back to the time domain:

$$\left.\frac{d\bar{\Theta}}{dz}\right|_{z=1}=-\frac{1}{s}-\frac{1}{\sqrt{s}}.\tag{A.8}$$

Using tables of the inverse Laplace transformation (e.g. [6]) yields

$$\left.\frac{d\Theta}{dz}\right|_{z=1}=-\left(1+\frac{1}{\sqrt{\pi\tau}}\right).\tag{A.9}$$

Now, the transient Nusselt number as given in Eq. (9) is obtained:

$$\mathrm{Nu}=\frac{hd}{k}=\frac{d}{T_\infty-T_\mathrm{d}}\left.\frac{\partial T}{\partial r}\right|_{r=R}=-2\left.\frac{\partial\Theta}{\partial z}\right|_{z=1}=2\left(1+\frac{1}{\sqrt{4\pi\,\mathrm{Fo}_0}}\right).\tag{A.10}$$

Note that the Fourier number Fo_0 is calculated with the droplet diameter, however, the dimensionless time τ used here is formulated with the droplet radius, thus $\tau=4Fo_0$.

Appendix B. Derivation of Eq. (14)

Here, the energy equation for the transient gas phase around a stagnant droplet is derived. In spherical coordinates, the conservation equation reads (e.g. [4]):

$$\varrho c_p\frac{\partial T}{\partial t}=k\frac{1}{r^2}\frac{\partial T}{\partial r}\left(r^2\frac{\partial T}{\partial r}\right)+\varrho c_p u_r\frac{\partial T}{\partial r}.\tag{B.1}$$

The radial velocity can be computed from the droplet mass:

$$\dot{u}_r=-\frac{1}{4\pi\varrho r^2}\frac{\partial m}{\partial t}=-\frac{\dot{m}''}{\varrho}\frac{R^2}{r^2}\tag{B.2}$$

with the surface mass flux $\dot{m}''$ (Eq. (15)).

Introducing a dimensionless radial coordinate $z=r/R(t)$ with the time-dependent droplet radius $R(t)$ yields the following substitutes for the differential operators:

$$\begin{aligned}&\frac{\partial}{\partial t}=\frac{\partial}{\partial t}+\frac{\partial}{\partial z}\cdot\frac{\partial z}{\partial t}=\frac{\partial}{\partial t}-\frac{\partial}{\partial z}\cdot\frac{r}{R^2}\frac{dR}{dt}=\frac{\partial}{\partial t}-z\frac{\dot{R}}{R}\frac{\partial}{\partial z},\\&\frac{\partial}{\partial r}=\frac{\partial}{\partial z}\cdot\frac{\partial z}{\partial r}=\frac{1}{R}\frac{\partial}{\partial z}\end{aligned}\tag{B.3}$$

with $\dot{R}=dR/dt$.

Thus, the transformed differential equation is obtained:

$$\varrho c_p\left(\frac{\partial T}{\partial t}-z\frac{\dot{R}}{R}\frac{\partial T}{\partial z}\right)=k\frac{1}{R^3z^2}\frac{\partial T}{\partial z}\left(z^2R\frac{\partial T}{\partial z}\right)-c_p\frac{\dot{m}''}{z^2}\frac{1}{R}\frac{\partial T}{\partial z}.\tag{B.4}$$

Rearranging the terms yields Eq. (14):

$$\varrho c_p\left(\frac{\partial T}{\partial t}-z\frac{\dot{R}}{R}\frac{\partial T}{\partial z}\right)=k\frac{1}{R^2z^2}\left(2z\frac{\partial T}{\partial z}+z^2\frac{\partial^2T}{\partial z^2}\right)-c_p\frac{\dot{m}''}{z^2}\frac{1}{R}\frac{\partial T}{\partial z},\tag{B.5}$$

$$\frac{\partial T}{\partial t}=\left(\frac{k}{\varrho c_p}\frac{2z}{R^2z^2}-\frac{\dot{m}''}{z^2\varrho R}+z\frac{\dot{R}}{R}\right)\frac{\partial T}{\partial z}+\frac{1}{R^2}\frac{k}{\varrho c_p}\frac{\partial^2T}{\partial z^2},\tag{B.6}$$

$$\frac{\partial T}{\partial t}-\left(z\frac{\dot{R}}{R}-\frac{\dot{m}''}{z^2\varrho R}+\frac{2\alpha}{zR^2}\right)\frac{\partial T}{\partial z}-\frac{\alpha}{R^2}\frac{\partial^2T}{\partial z^2}=0.\tag{B.7}$$

The equation for the mass fraction is derived analogically by replacing T and α by ξ and D. The correlations for the temperature and concentration within the droplet follow from Eq. (B.7) by setting $\dot{m}''=0$.

References

[1] B. Abramzon, W.A. Sirignano, Droplet vaporization model for spray combustion calculations, Int. J. Heat Mass Transfer 320 (9) (1989) 1605–1618.
[2] S.K. Aggarwal, G.-S. Zhu, R.D. Reitz, Quasi-steady high-pressure droplet model for diesel sprays, SAE Technical Paper 2000-01-0588, 2000.
[3] K. Anders, N. Roth, A. Frohn, Simultaneous in situ measurements of size and velocity of burning droplets, Part. Part. Syst. Charact. 8 (1991) 136–141.
[4] R.B. Bird, W.E. Stewart, E.N. Lightfoot, Transport Phenomena, Wiley, New York, 1960.
[5] H. Brauer, Grundlagen der Ein- und Mehrphasenströmungen, Sauerländer, Aarau, 1971.
[6] I.N. Bronstein, K.A. Semendjajew, G. Musiol, H. Mnhlig, Taschenbuch der Mathematik, Verlag Harri Deutsch, Frankfurt am Main, Thun, 14th ed., 1998.
[7] G. Castanet, M. Lebouche, F. Lemoine, Heat and mass transfer of combusting monodisperse droplets in a linear stream, Int. J. Heat Mass Transfer 48 (2005) 3261–3275.
[8] C.H. Chiang, W.A. Sirignano, Interacting convecting vaporising fuel droplets with variable properties, Int. J. Heat Mass Transfer 360 (4) (1993) 875–886.
[9] T.E. Daubert, R.P. Danner, Physical and Thermodynamic Properties of Pure Chemicals Data Compilation, Hemisphere, New York, 1989.
[10] FLUENT 6.0, Fluent 6.0 Users Guide, Fluent Inc., Lebanon, NH, USA, 2002.
[11] N. Frössling, Über die Verdunstung frei fallender Tropfen, in: Gerlands Beiträge zur Geophysik, 1938, pp. 170–215.
[12] J. Gmehling, B. Kolbe, Thermodynamik, second ed., VCH Verlagsgesellschaft, Weinheim, 1992.
[13] S. Hohmann, Strahlausbreitung und Tropfenverdunstung bei der dieselmotorischen Direkteinspritzung, Ph.D. Thesis, RWTH Aachen, 1999. ISBN 3-8265-6246-1.
[14] S. Hohmann, U. Renz, Numerical simulation of fuel sprays at high ambient pressure: the influence of real gas effects and gas solubility on droplet vaporisation, Int. J. Heat Mass Transfer 46 (2003) 3017–3028.
[15] G.L. Hubbard, V.E. Denny, A.F. Mills, Droplet evaporation: effects of transients and variable properties, Int. J. Heat Mass Transfer 18 (1975) 1003–1008.
[16] M. Klingsporn, U. Renz, Vaporization of a binary unsteady spray at high temperature and high pressure, Int. J. Heat Mass Transfer 37 (Suppl. 1) (1994) 265.
[17] R. Kneer, M. Willmann, M. Schnieder, D. Hirleman, R. Koch, S. Wittig, Theoretical studies on the influence of reactive index gradients within multicomponent droplets on size measurements by phase doppler anemometry, in: ICLASS-94 Rouen, France, July 1994, p. 451.
[18] D. Liu, K. Anders, A. Frohn, Drag coefficient of single droplets moving in an infinite droplet chain on the axis of a tube, Int. J. Multiphase Flow 140 (2) (1988) 217–232.

[19] R.S. Miller, K. Harstad, J. Bellan, Evaluation of equilibrium and non-equilibrium evaporation models for many-droplet gas–liquid flow simulations, Int. J. Multiphase Flow 24 (1998) 1025–1055.
[20] W. Ranz, W. Marshall, Evaporation from drops, Part I, Chem. Eng. Prog. 480 (3) (1952) 141–146.
[21] L. Reichelt, Aerodynamischer Tropfenzerfall bei dieselmotorischen Umgebungsbedingungen, Ph.D. Thesis, RWTH Aachen, 2004. ISBN 3-8322-2954-X.
[22] R.C. Reid, J.M. Prausnitz, B. Poling, The Properties of Gases and Liquids, fourth ed., McGraw-Hill, New York, 1987.
[23] N. Roth, K. Anders, A. Frohn, Mutual interaction between burning aerosol droplets in the micrometer range, J. Aerosol. Sci. 200 (8) (1989) 991–994.
[24] M. Staudt, U. Meingast, U. Renz, Ansaugverhalten von Common-Rail-Einspritzstrahlen bei verdunstenden Bedingungen und Wandeinfluss, in: Spray 2001, TU Hamburg Harburg, 2001.